Langmuir

Article

pubs.acs.org/Langmuir

Thermocapillary Flow in Glass Tubes Coated with Photoresponsive Layers

J. Rodrigo Vélez-Cordero,* A. M. Velázquez-Benítez, and J. Hernández-Cordero

Instituto de Investigaciones en Materiales, Universidad Nacional Autónoma de México, Apdo. Postal 70-360, México D.F. 04510, México

ABSTRACT: Thermocapillary flow has proven to be a good alternative to induce and control the motion of drops and bubbles in microchannels. Temperature gradients are usually established by implanting metallic heaters adjacent to the channel or by including a layer of photosensitive material capable of absorbing radiative energy. In this work we show that single drops can be pumped through capillaries coated with a photoresponsive composite (PDMS + carbon nanopowder) and irradiated with a light source via an optical fiber. Maximum droplet speeds achieved with this approach were found to be ~300 μm/s, and maximum displacements, around 120% of the droplet length. The heat generation capacity of the coatings was proven having either a complete coating over the capillary surface or a periodic array of pearls of the photoresponsive material along the capillary produced by the so-called Rayleigh−Plateau instability. The effect of the photoresponsive layer thickness and contact angle hysteresis of the solid−liquid interface were found to be important parameters in the photoinduced thermocapillary effect. Furthermore, a linear relationship between the optical intensity I_o and droplet velocity v was found for a wide range of the former, allowing us to analyze the results and estimate response times for heat transfer using heat conduction theory.

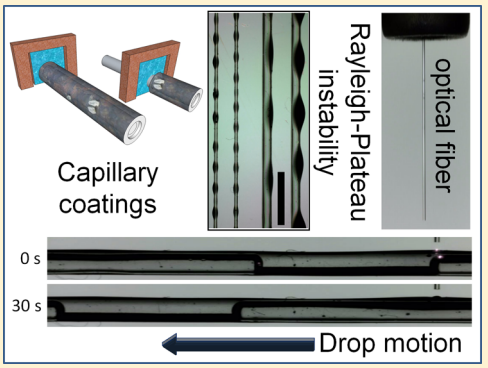

INTRODUCTION

The conversion of radiative optical power into a mechanical rate of work (or simply the conversion of "light to work", see the illustrative paper of Okawa et al.[1]) is a topic that has brought about new research areas in the field of micro- and nanofluidics, greatly enriching the so-called low Reynolds number hydrodynamics. Nowadays, researchers make references to optofluidics—the interaction of light in micro- and nanoscale fluids[2,3]— optoelectrowetting and digital microfluidics,[2,4] optohydrodynamic instabilities mediated by radiative pressure in ultralow surface tension interfaces,[5] optomechanics,[6,7] optothermorheological flows, where the rheology of polymers is changed on demand by applying heat,[8,9] and the widespread technique known as optical tweezers,[10] to name a few. The conversion of light to work, either by transferring energy through different heat-transfer modes, direct moment transfer from the light beam, or light interaction at the chemical bonding−structure level, is so versatile that there is increasing interest in manipulating fluids using mainly optical, or radiative, power (i.e., the totally optical lab on a chip[5]). Such an interest is not just academic since sunlight is by far the most abundant energy source and could provide unlimited power to microfluidic devices. Baigl and Chen et al.[2,11] have recently reviewed the ongoing research concerning optofluidic devices and its applications.

The manipulation of microbubbles and drops in closed environments using optofluidics has attracted particular attention due to their employment in biological and chemical experiments.[12,13] Similar setups with adjustable parameters and configurations (the position of the laser beam, for example) can work as distinct operational units such as mixing, valves, dispersion, splitting, fusion, sorting, and so forth, all of which can be used as building blocks, in a certain sequence, to conform a whole process at the lab-on-a-chip scale.[2,5,12−15] We can therefore expect that some of these operational units, which currently work with mechanical pumps, will eventually be assisted partially or totally by optical power.

Different strategies have been offered to convert light into work; most of the reported setups have been developed to produce the motion of sessile drops on different substrates or the motion of bubbles or drops immersed in a secondary fluid inside microchannels.[16−21] In all of these cases, energy conversion is achieved via light absorption leading either to conformational changes on the molecular level or to thermal effects. Drop motion driven by thermal effects is usually achieved by using a host medium with embedded particles that absorb light at a certain wavelength.[2,5,15,17,20,22] The subsequent rise in temperature can be used to change either the bulk properties or induce phase transitions[19,23] or to change the interfacial properties of the material in order to induce motion. Thermocapillary flow assisted by photoirradiation has already been used to move air bubbles[17] and drops[20] at velocities comparatively larger than those achieved by other methodologies (maximum speeds of 1.5 to 3 mm/s). Other works have

Received: November 1, 2013
Revised: February 10, 2014
Published: April 14, 2014

   dx.doi.org/10.1021/la404221p | *Langmuir* 2014, 30, 5326−5336

reported more sophisticated liquid−liquid or liquid−solid interface motions by inducing thermocapillary flow coupled with thermophoresis or solutocapillary effect.[15,24,25]

In this paper we present a study of the thermocapillary flow of a single drop inside a microchannel induced by photo-irradiation. Unlike previous works where the absorbing material was placed as part of the layers forming the microdevice (square channel geometry), here we demonstrate that heat flux can be generated and transferred by coating a capillary glass (cylindrical channel geometry) with the photoresponsive material. The motion of the drops is discussed around three main aspects: contact angle hysteresis, layer thickness of the absorbing material, and the preferential mode (conduction or radiative) used for heat transfer. Basic considerations of these aspects and their respective contribution to drop motion are mentioned in the following sections.

Thermocapillary Flow and Contact Angle Hysteresis. The thermocapillary motion of single drops has been demonstrated by Sammarco and Burns[26] using a microchannel equipped with patterned heaters. Consider the motion of a drop of length L inside a cylindrical channel with diameter d, as shown in Figure 1. When the drop is at rest, both menisci have

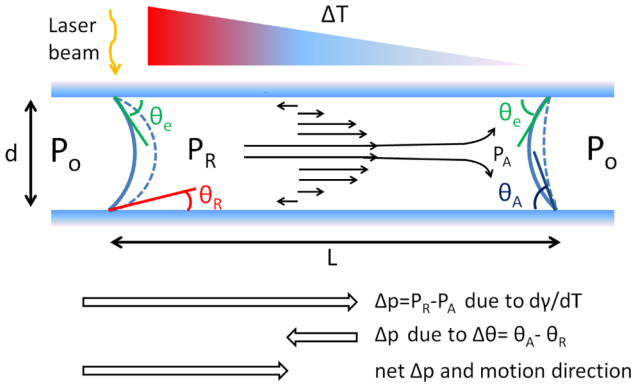

Figure 1. Schematic representation of the drop motion activated by the thermocapillary effect. A temperature gradient ΔT produces an overall pressure difference $\Delta P = P_R - P_A$ due to the surface tension dependence on temperature, $d\gamma/dT$. If instead of considering an equal contact angle θ_e at both menisci we take into account a contact angle hysteresis $\Delta\theta = \theta_A - \theta_R$, where θ_A and θ_R correspond to the advancing and receding contact angles, respectively, then a pressure difference is established opposed to that imposed by the thermocapillary effect. The latter usually overcomes the hysteresis effect, and a net flow is observed toward the colder region (higher surface energy). The lines in the figure represent the fluid flow inside the drop, d and L are the diameter of the tube and length of the drop, respectively, and subscripts A and R denote the advancing and receding sides of the droplet.

the same static contact angle θ_e (solid line in Figure 1). Upon increasing the temperature T on one of the extremes of the drop (left meniscus in Figure 1), the surface tension γ will decrease according to the equation of state $\gamma = a - bT$, where a/b [N m^{-1}/N (m °C)$^{-1}$] is a critical thermodynamic point.[26] The Young−Laplace law states that the reduction of the surface tension at this interface will reduce the pressure difference between the reference pressure P_o and the liquid pressure P_R on this side according to $P_o - P_R = 4\gamma \cos\theta_e/d$.

Within the drop, a global $\Delta P = P_R - P_A$ is then established, which is the condition to induce mean fluid motion to the right (Figure 1) according to[26]

$$v = \left(\frac{d^2}{32\mu L}\right)\Delta P \tag{1}$$

where μ is the liquid viscosity. Note that this equation assumes that the pressure difference produces a Poiseuille flow inside the drop, as depicted in Figure 1; such a velocity profile clearly breaks near the edges where convective streamlines appear due to momentum conservation.[27] In the limit when $L/d \gg 1$, the convective patterns at both edges can be assumed to be negligible.

The drop shape in this scenario produces a velocity that is proportional to ΔT since both the flow velocity and the equation of state are linear relations. However, unless there is an equal relative slip at both triple contact lines (i.e., at the advancing and receding sides of the drop), the initial curvatures will bend until reaching the final dynamic contact angles (dashed lines in Figure 1). According to the Laplace law this final configuration will actually induce a pressure difference opposite to that produced by the reduction of the surface tension on the receding site, and the larger the difference between the receding and advancing contact angles $\Delta\theta = \theta_A - \theta_R$, the larger the motion resistance will be. Therefore, the contact angle hysteresis $\Delta\theta$ represents a kind of activation energy that needs to be supplied in order to start up the motion of the drop. Sammarco and Burns[26] derived the velocity equation by taking into account this consideration, which for circular ducts has the form

$$v = \frac{4}{32}\frac{d}{L}\frac{b\cos\theta_R}{\mu}(\Delta T - \Delta T_{min}) \tag{2}$$

where $\Delta T = T_R - T_A$, with T_R being the temperature at the receding site and T_A being the temperature at the advancing site, usually taken as the reference temperature, and

$$\Delta T_{min} = \left(\frac{a}{b} - T_A\right)\left[1 - \frac{\cos\theta_A}{\cos\theta_R}\right] \tag{3}$$

is the minimum temperature difference needed to set the drop into the final configuration and initiate thermocapillary pumping; therefore, the wetting properties of the drop on a solid surface become crucial in these kind of flows. The contact angle hysteresis is a well -documented phenomenon in the literature, and different strategies have been proposed to reduce its effects in different solid−liquid combinations.[28−30]

Photoresponsive Layer Thickness. Our approach for inducing the temperature gradient required to induce thermocapillary flow is based on coating capillary tubes with the light-absorbing material; hence, heat not only has to be generated but also transmitted to the inner part of the tube. In absorbing materials, it is common to refer to the optical length as $\tau_\lambda = \beta_\lambda h$, where β_λ is the extinction coefficient of the medium at a certain wavelength (λ) and h is the thickness of the material. In general, for very low values of τ_λ, the material will produce low heat per unit volume while a very large τ_λ will produce high temperatures at the surface facing the light source but low temperatures in deeper layers; therefore, an intermediate τ_λ is expected to be the optimum value. The thickness h of the layer obtained when coating a capillary tube at a coating velocity U in the longitudinal direction can be estimated from fiber coating theory as[31,32]

$$h = 1.34rCa^{2/3} \tag{4}$$

dx.doi.org/10.1021/la404221p | Langmuir 2014, 30, 5326−5336

where r is the radius of the fiber or capillary and $Ca = \mu U/\gamma$ is the capillary number. Equation 4 is known as the Landau–Levich–Derjaguin equation (LLD theory) and is valid for $Ca \ll 1$.[32] The dependence of h on the capillary number arises from the antagonist roles of viscous and capillary forces:[32] while the solid surface drags the fluid at a velocity U (considering the no-slip condition), the surface tension of the liquid tends to oppose such flow due to the deformation at the liquid surface.

If the photoresponsive material solidifies rapidly, then h will be the final thickness over the entire capillary surface. If this is not the case, then the liquid surface will tend to undulate and finally break into a periodic array of droplets or pearls; this surface-tension-driven instability is the well-known Rayleigh–Plateau instability.[32,33] Such an instability obeys a minimization surface energy principle, and it is always seen that very small disturbances (perturbations), in our case, those produced by the coating process, grow in amplitude at a certain rate. Using the lubrication approximation, Dumbleton and Hermans[34] determined that the characteristic growth time for the most unstable perturbation of a thin annular layer is given by

$$t^* = 12\frac{\mu(r+h)^4}{\gamma h^3} \tag{5}$$

corresponding to a perturbation having a wavenumber of

$$q^* = \frac{2\pi}{\lambda} = \frac{1}{\sqrt{2}\,(r+h)} \tag{6}$$

Equation 5 states that we can control the characteristic time t^* of the instability by varying the layer thickness h obtained during the coating process: for low values of h, a small cross-sectional area is left for the coating to flow, and the characteristic growth time will be large; the opposite will happen for larger values of h where eq 5 will give the right t^* provided that the lubrication approximation is not violated.

Heat Transfer in Semitransparent Media. Another important ingredient considered in this report deals with the generation and heat transfer in semitransparent media. Our interest here is to identify the heat-transfer modes that are active during the photoirradiation of the photoresponsive material, where the relation between ΔT and the optical intensity I_o (optical power per unit area) must be determined. When the beam enters the medium, light can be either absorbed or scattered, leading to an exponential decay of the optical density $I(\tau)/I_o = e^{-\tau_\lambda}$ (note that for $\tau_\lambda = 2.3$, the optical intensity has decreased 90%). Optical absorption contributes to the heat flux transferred throughout the medium by conduction, emission (radiation), or convection. In the case of solid materials, the relative importance of conductive and radiative heat fluxes can be estimated with the conduction-to-radiation parameter[35,36]

$$N = \frac{k\kappa_{abs}}{4\sigma T^3} \tag{7}$$

where k is the thermal conductivity of the material, κ_{abs} is the absorption coefficient, σ is the Stefan–Boltzmann constant (5.67^{-8} W/m^2 K^4), and T the local temperature of the medium. For $N \to \infty$, the conduction of heat transfer dominates and the spatial temperature gradient ΔT is proportional to I_o. If the temperature of the medium is such that $N < 1$, then the heat flux due to conduction will be coupled with the radiative heat equation, which leads to a nonlinear relation between the temperature and I_o. In the present investigation we worked at room temperature (27 °C), so essentially internal emission from the photoresponsive material will not occur, and we expect to recover the linear relationship between the droplet velocity and the optical intensity, $v \propto I_o$.

EXPERIMENTAL SECTION

In this section we first describe the methodology used to coat the capillaries with and without the formation of a periodic array of pearls generated by surface instabilities. We then describe the selection of the liquid based on a low contact angle hysteresis criterium followed by the experimental setup.

Capillary Tubes and Coating Methodology. We selected two capillaries with small wall thicknesses in order to minimize the heat-transfer resistance. The dimensions of the capillary tubes were the following: Drummond capillary (further denoted by CAP135), 135.9 μm wall thickness, 314.95 μm inner radius, 6.4 cm length; TrianaTech capillary (further denoted as CAP65), 65 μm wall thickness, 100 μm inner radius, 4.1 cm length.

The photoresponsive composite was made by mixing 2.4 ± 0.2 mg/g of carbon nanopowder (<50 nm, Adrich 633100) in poly(dimethylsiloxane) (PDMS-Sylgard 184 from Dow Corning) that is 1:10 with respect to curing agent. The composite was mixed by hand until an average carbon cluster size of about 30 μm was achieved. (This value was determined by making a thin membrane of the composite and analyzing a magnified image with Matlab.) The physical properties considered for the PDMS were ρ = 965 kg/m^3, μ = 3.9 Pa·s, and γ = 19.8 mN/m.[36b,37] The extinction coefficient of photoresponsive materials is a function of the nanopowder concentration. Increasing the powder concentration is equivalent to increasing the thickness h of the layer by virtue of the definition of the optical length; therefore, in the present work we used a single concentration value, and no attempt was made to study the dependence of the drop velocity on the nanopowder concentration.

The capillaries were coated with the photoresponsive composite in a horizontal motorized stage, as sketched in Figure 2a. Such a device was primarily designed to coat optical fibers; therefore, in order to place the capillaries firmly in the coating apparatus, optical fibers were threaded inside the tubes. Next, both ends of the capillaries were sealed by putting a small amount of silicon sealant (Sista, Dow Corning, general purpose) to avoid the filtration of the photoresponsive material.

A grooved transverse bar made of PTFE is then placed at one extreme of the capillaries (see Figure 2a); the capillaries pass through this groove (with a cross-sectional area of 1.5 × 2 mm^2 and a width of 6.5 mm) used as reservoir for the photoresponsive material. Once the photoresponsive composite is poured into the groove, the capillary is coated using a motor to move the bar at a constant speed U along the full length of the tube. A heater is then placed on top of the capillary, and the composite is left to cure for 2 h at 75 °C. If the surface instability is allowed to form, then the polymer is left at room temperature until the pearls are formed and then it is heated for 2 h. When this process is completed, the silicon seals and the fiber are removed from the capillaries.

Working Fluid and Contact Angle Hysteresis. The contact angle hysteresis $\Delta\theta = \theta_A - \theta_R$ constitutes a crucial parameter in thermocapillary pumping. One way to estimate the value of $\Delta\theta$ is by placing a drop on a goniometer and then tilting the surface until the drop starts moving. A force balance can be used to show[38] that the angle ϕ at which the drop moves can be estimated as

$$\pi r_{line}\gamma(\cos\theta_R - \cos\theta_A) = \rho V g \sin\phi \tag{8}$$

where V is the volume of the drop, g is gravity, and r_{line} is the radius of the triple contact line, here considered to be circular and in which the upper half of the droplet has a contact angle θ_R and the lower half has a contact angle θ_A. Table 1 shows the angle ϕ together with the static contact angle θ_e measured for several liquid–solid combinations: distilled water and mineral oil drops having a volume V = 15.76 ± 0.1 μL were placed on clean glass and glass treated with polysiloxanes to make it hydrophobic. Since PDMS is commonly used to make

dx.doi.org/10.1021/la404221p | Langmuir 2014, 30, 5326–5336

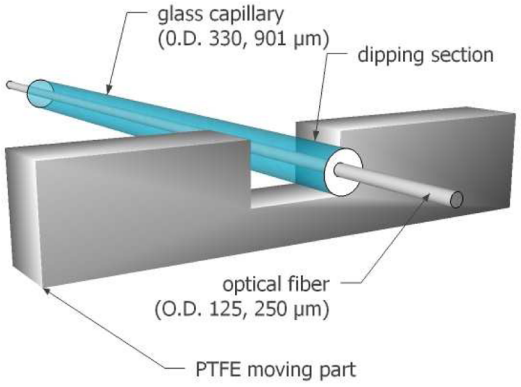

(a)

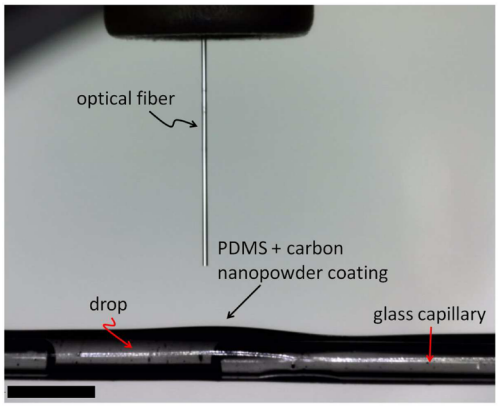

(b)

Figure 2. Experimental setup. (a) Sketch of the coating process: the capillaries are placed inside the grooves of the transverse bar and fixed at the extremes with an optical fiber, and the bar then moves in order to coat the entire capillary surface with the liquid composite. (b) In order to produce the thermocapillary flow, a section of the coated capillary is photoirradiated with an optical fiber placed perpendicular to it; the scale bar is 2 mm.

microchannels, we compared the characteristic angles found in glass to those measured on a cured PDMS membrane. The static contact angle was measured by fitting a circle around the drop and then drawing the tangent line at one of the triple contact points (image processing was carried out in Matlab, six different measurements were made for each solid–liquid interface). The values measured for θ_e were compared to the geometrical relations given by Quéré[38]

$$\delta = 2\left(\frac{3}{\pi}\right)^{1/3} \frac{\sin\theta_e}{(2+\cos\theta_e)^{1/3}(1-\cos\theta_e)^{2/3}} V^{1/3} \quad (9)$$

for $\theta_e < 90°$ and

$$\delta = 2\left(\frac{3}{\pi}\right)^{1/3} \frac{1}{(2+\cos\theta_e)^{1/3}(1-\cos\theta_e)^{2/3}} V^{1/3} \quad (10)$$

for $\theta_e < 90°$, where δ is the diameter of the drop as seen from above.

As seen in Table 1, both methods can be used to estimate θ_e, with the maximum difference being 10% for hydrophobic surfaces. We classified the liquid–solid pairs according to the angle ϕ: glass–oil, PDMS–oil, and hydrophobic glass–water interfaces have low ϕ (i.e., low contact angle hysteresis). On the other hand, for the same given volume V, glass–water and PDMS–water interfaces have relatively higher contact angle hysteresis: most of the drops stayed attached to the surface at $\phi = 90°$. Note that even for the PDMS–water system in which $\theta > 90°$ (low wetting surface) the contact angle hysteresis is large. In the particular case of the PDMS–mineral oil pair, we observed a rapid absorption of the oil into the polymeric matrix. There are several strategies reported in the literature to reduce the contact angle hysteresis in glass, PDMS, or another kind of surface.[29,39−41] Here our interest is to use pristine liquid–solid interfaces with the lowest $\Delta\theta$, in our case, the glass–mineral oil pair.

Thermocapillary Pumping Setup. For the thermocapillary pumping experiments, we placed a drop inside the capillaries, typically 3.8 mm long (0.12 and 1.18 μL for the CAP65 and CAP135 capillaries, respectively). A laser diode (λ = 975 nm, 200 mW maximum output power) coupled to an optical fiber was used as the light source. In order to ensure a single-mode output with a Gaussian intensity profile, a mode stripper was used near the output end of the optical fiber. The fiber (Corning SMF-28e, NA = 0.14) was placed perpendicular to the capillary surface (see Figure 2b) with the help of a manual stage at a fixed position and distance from the capillary (316 ± 6 μm) to irradiate the same area in all cases. Since the angle of acceptance is equal to $\sin^{-1}$(NA), the estimated irradiated area was ∼5996 μm^2. A digital microscope (Dino-Lite AD7013MZT) was used to obtain videos of the moving droplets, in which the typical resolution was 6 μm/pixel. The velocity measurements were made in *ImageJ*, and the position versus time for each meniscus was registered to obtain separate measurements of the velocity at both extremes of the drop.

RESULTS

Coating Experiments: The Multilayer Procedure. We observed that the annular layer of the photoresponsive material is highly prone to surface perturbations during the coating procedure. In order to obtain a layer with relatively low surface instabilities, eq 5 dictates that a small layer thickness h has to be applied along the capillary (i.e., low-speed coatings according to eq 4). For the wider capillary, CAP135, we repeated the coating

Table 1. Experimental and Theoretical Static Contact Angles θ_e and Tilt Angles ϕ for Different Solid–Liquid Interfaces[a]

Interface	Exp. θ_e	θ_e from eq.9 or 10	Tilt angle ϕ	
Adequate solid-liquid interface for Marangoni flow				
glass-mineral oil	9.0 ± 0.86°	8.0 ± 0.61°	∼ 2.0°	
PDMS-mineral oil	36.1 ± 2.59°	35.7 ± 2.4°	10.0 ± 2.16°	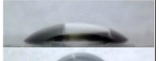
glass/polysiloxanes-water	95.9 ± 2.44°	86.2 ± 1.6°	13.0 ± 8.0°	
Inadequate solid-liquid interface for Marangoni flow				
glass-water	48.3 ± 5.07°	50.7 ± 5.9°	(4) no slip, (2) ∼ 54°	
PDMS-water	103.3 ± 5.95°	95.1 ± 5.61°	no slip	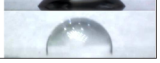

[a]The volume of the drop V was fixed in all cases: 15.76 ± 0.1 μL. For reference, $\delta/2$ for the glass–water interface has the same value as the capillary length for water $k_{cap}^{-1} = (\gamma/\rho g)^{1/2}$ = 2.7 mm. For the glass–water interface, four out of six drops stayed attached to the drop at $\phi = 90°$ while for the PDMS–water pair all six drops remained attached at $\phi = 90°$.

dx.doi.org/10.1021/la404221p | *Langmuir* 2014, 30, 5326−5336

process several times (multilayers), each time increasing the layer thickness by a factor of around 1.6. The coating velocity for this case was set to 5.21 mm/min (Ca = 0.01), which according to eqs 4 and 5 yields a characteristic time of t^* = 35 min for the most unstable wavenumber. Calculations using the full solution of the axisymmetric instability of an annular thread with negligible inertia[42] yields the same time. This characteristic time is in the order in which the PDMS starts to solidify at 75 °C. Figure 3 shows pictures of CAP135 capillaries for each

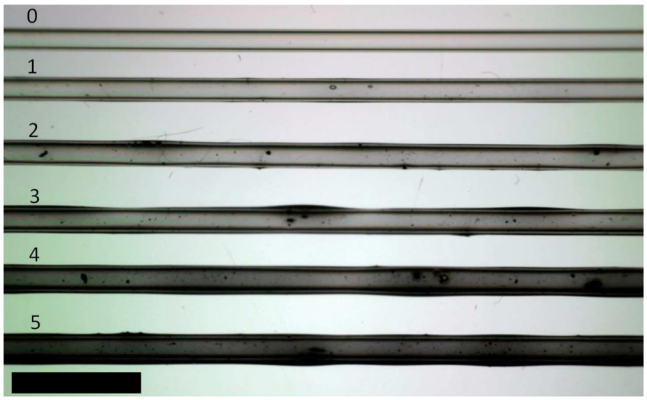

Figure 3. Photograph of the CAP135 capillaries coated with the photoresponsive composite using a multilayer procedure. The numbers denote the coating step; the coating velocity was U = 5.21 mm/min. The scale bar is 5 mm.

coating step (up to five coating steps, denoted in the figure by numbers). The PDMS + nanocarbon composite covers the entire surface, although it is evident that variations in the thickness develops due to the instability. A more homogeneous surface could be achieved if the coating velocity is reduced even more (although this will lead to a very slow rate of increase in h) or if heating is applied while coating to speed up solidification of the photoresponsive material. Although the effects of gravity and inertia can be considered to play a negligible role in the final value of h (the Bond $Bo = \rho g r^2/\gamma$ and Weber $We = \rho U^2 r/\gamma$ numbers are 0.1 and 1.7 × 10^{-7}, respectively), we did notice a slight asymmetry in the thickness of the layer due to gravity during the 2 h solidification period.

Figure 4 shows the accumulated thickness h of the composite layer for each coating step. The error bars reflect the thickness variance obtained from 11 measurements made at different sites for each capillary; the value of h according to the LLD theory, eq 4, is also shown. Although experiments and theory closely followed the same trend, the LLD coating law predicts a higher accumulated thickness h, and its slope in Figure 4 is clearly higher after the third coating step with respect to the experimental values. The difference may be due to the fact that the LLD theory considers a no-slip condition between the solid surface and the liquid, a condition which is not strictly rigorous in smooth or noninteracting surfaces. It has been shown[43] that slippage between the solid and liquid in these systems yield lower values of h since the interface "feels" a lower viscosity due to the slip condition. The disagreement of the experimental values from the classic LLD theory suggest then that, unlike the glass−PDMS interface, the PDMS(solid)−PDMS(liquid) interface, which is in fact the contact surface after the first coating step, has some degree of slippage. Following Liao et al.,[43] an apparent viscosity, $\mu_{app} = \mu h/(h + \lambda_{slip})$, was considered in this case, where λ_{slip} is the slip length

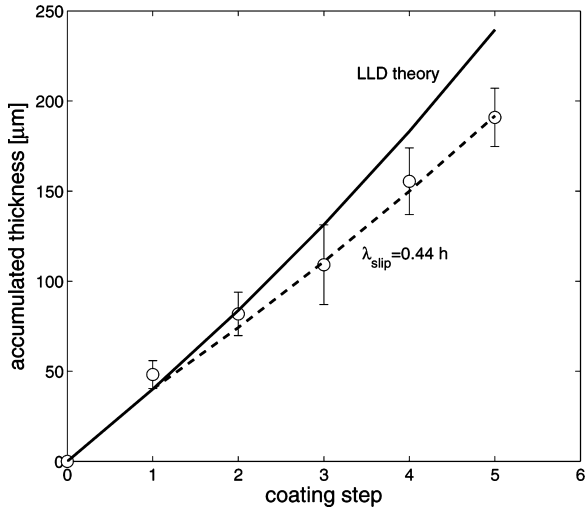

Figure 4. Accumulated thickness h of the photoresponsive layer at each coating step in the multilayer procedure: (○) experiments, the solid line denotes the theoretical value computed with eq 4, the dotted line indicates the modified LLD theory considering a slip length of λ_{slip}/h = 0.44. The error bars represents the deviation from the mean obtained from 11 measurements of h at different sites on the capillaries.

and is included in eq 4 to compute the capillary number. The dotted line in Figure 4 denotes the modified LLD theory, which fits the experimental data by considering a ratio $\lambda_{slip}/h = (\mu/\mu_{app}) - 1 = 3.9/2.7-1 = 0.44$, starting after the first coating step.

Coating Experiments: Design of a Pattern of Heaters via Surface Instabilities. In principle, the thinner capillaries (CAP65) can also be coated by employing a multilayer procedure. This time, however, we will need to increase the composite layer at a rate of ∼10 μm for each coating step in order to match the characteristic growth time of the instability with the polymer solidification time. Alternatively, we can coat the CAP65 capillaries at higher speeds, allowing the instability to grow until saturation (i.e., until a pattern array of pearls is fully developed). Figure 5 shows pictures of four capillaries

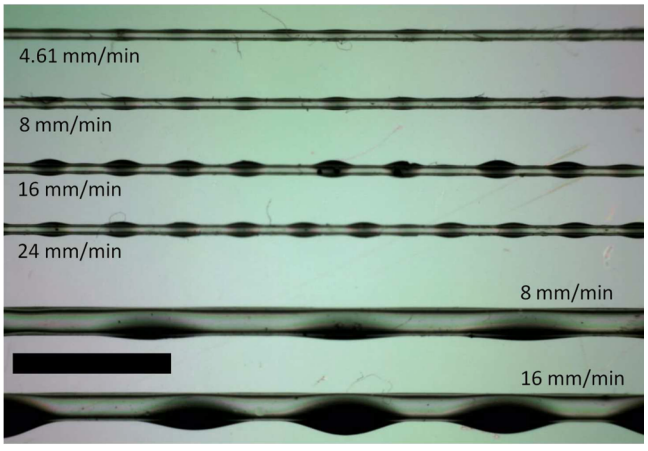

Figure 5. Photograph of the CAP65 (top four) and CAP135 capillaries coated with the photoresponsive composite at different coating velocities in a single step. The Rayleigh−Plateau instability is allowed to form. The numbers denote the coating velocity. The scale bar is 5 mm.

dx.doi.org/10.1021/la404221p | Langmuir 2014, 30, 5326−5336

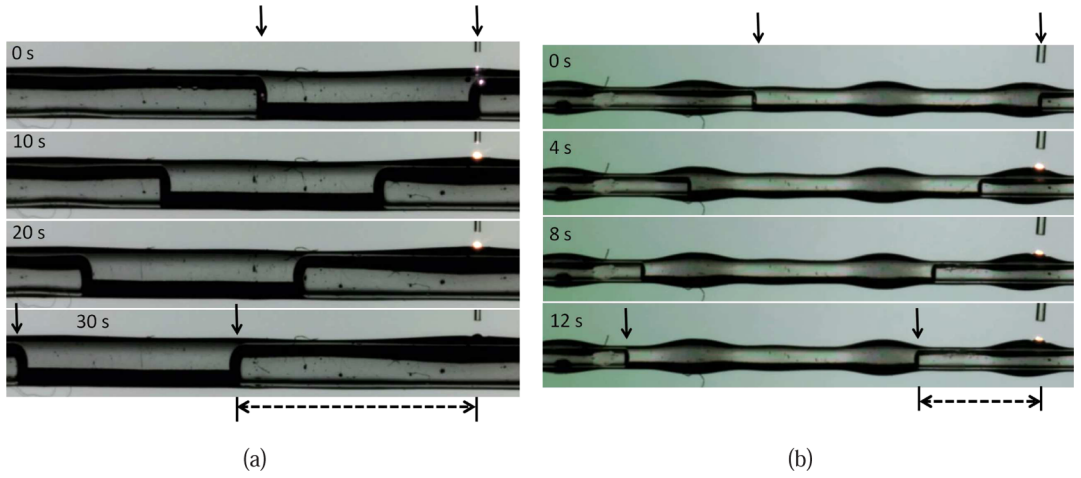

Figure 6. Sequence of the drop displacement along the capillaries: (a) drop inside the CAP135 capillary, $\overline{v}_{max}$ = 223 μm/s, optical power of 146.7 mW, h = 163 μm, drop size 4.05 mm (1.26 μL); (b) drop inside the CAP65 capillary, $\overline{v}_{max}$ = 241 μm/s, optical power of 109 mW, pearl thickness h = 130 μm, drop size 3.9 mm (0.12 μL). Photoirradiation on the surface can be observed by the light spot in front of the optical fiber, which at these powers produce incandescence. The vertical lines denote the initial and final positions of the drop menisci; the horizontal dashed lines indicate the total displacement of the droplet. The reported thicknesses h were measured at the point of irradiation.

CAP65 and two capillaries CAP135 coated at different speeds and leaving a certain period of time afterwards for the instability to grow. The coating velocity of 24 mm/min (Ca = 0.07) for CAP65 corresponds, for example, to a characteristic growth time t^* of 1 min. (Goren's full solution[42] again agrees with the lubrication approximation.) Around 10 min after the coating process, the composite layer in this capillary has already developed a regular pattern of pearls over the entire capillary surface.

On the one hand, we can see that the spacing between the pearls developed in each capillary size, CAP65 and CAP135, does not change considerably with the increase in the coating velocity, although the periodicity between pearls does change for different capillary sizes. This is evident since $h < r$ for the coating velocity range tested in this work. Also note that the periodicity has a lower limit because the perturbations are stable for wavelengths smaller than the capillary circumference.[33] The mean experimental distance between pearls scales with the linear instability theory in eq 6: 1.8−2.2 mm for the CAP65 capillaries, where the theoretical values are $\lambda = 2^{3/2}\pi(r + h)$ = 1.5−1.8 and 5.5−6.3 mm for CAP165 and the theoretical values are 4.4−4.7 mm. On the other hand, the maximum thickness of the pearls does change significantly with the coating velocity as a result of the fact that more volume of the composite is available for each pearl due to the increase in h. For the CAP65 capillaries, the composite layer thickness was increased from 54 to 154 μm and in the CAP135 from 195 μm to 461 μm. As mentioned before, the Bond and Weber numbers are in all cases less than 1, although this time it is evident that symmetry breaking is driven by gravity, especially in the wider capillaries (Bo = 0.4 for CAP135, 16 mm/min).

Thermocapillary Flow Experiments: Drop Velocity Dependence on the Layer Thickness *h*. Figure 6 shows an example of the displacement of a mineral oil drop in a CAP135 capillary coated with the multilayer procedure and in a CAP65 capillary having a periodic array of composite pearls, in which the optical fiber is placed above one of them. Figure 7 shows the position of the advancing (filled symbols) and receding (empty symbols) menisci plotted as a function of time for three different values of h, expressed as the ratio $\chi = h/H$, where H is the thickness of the capillary wall. The lines on the figures represent the largest slope corresponding to the maximum velocity achieved by the drop. Naturally, as the drop moves away from the heat source (i.e., the irradiated region), ΔT decreases and so does the drop velocity.

In the Introduction we argue that optimal heat-transfer rates will be achieved at intermediate values of the optical length $\tau_\lambda = \beta_\lambda h$. For fixed values of β_λ, this means that maximum displacements and velocities of the droplet will be seen at intermediate values of the coating thickness h. This is clearly seen in Figure 7b for a CAP135 capillary, where the velocity and displacement first rise substantially as h increases (from χ = 0.34 to 1.2) and then decrease for thicker layers (χ = 3.4). In the case of the CAP65 capillaries, Figure 7c,d, only the range for the velocity decrement as a function of h was seen. In general, large displacements correspond to high velocities, although larger displacements were seen for capillaries coated completely with the multilayer procedure (χ = 1.2 case in Figure 7b), while higher velocities were seen for the CAP65 capillaries (i.e., when the characteristic time for heat transfer is smaller as the diameter of the capillaries and wall thickness are reduced (lines in Figure 7c,d)). The inset in Figure 7b shows the difference in the menisci velocities for the case when χ = 0.34, showing that drops moving slowly can undergo thermal expansion (as will happen if heat is applied at the center of the drop). Thermal expansion was typically 2.5%, with a single maximum point of 5.1% corresponding to that shown in the inset of Figure 7b.

Drop Velocity as a Function of the Optical Intensity. The maximum mean velocity (between the advancing and receding menisci) as a function of the optical intensity for the CAP135 capillaries coated with the multilayer procedure is shown in Figure 8. The solid line is a linear fitting curve for the maximum mean velocity, empty symbols denote those cases where incandescence was absent, and filled symbols denote those where incandescence was observed. The maximum velocity achieved without incandescence was 174 μm/s (maximum displacement was 120% of the drop length), and that with incandescence was 262 μm/s. Note that even when radiative heat transfer is present at the surface (i.e.,

dx.doi.org/10.1021/la404221p | Langmuir 2014, 30, 5326−5336

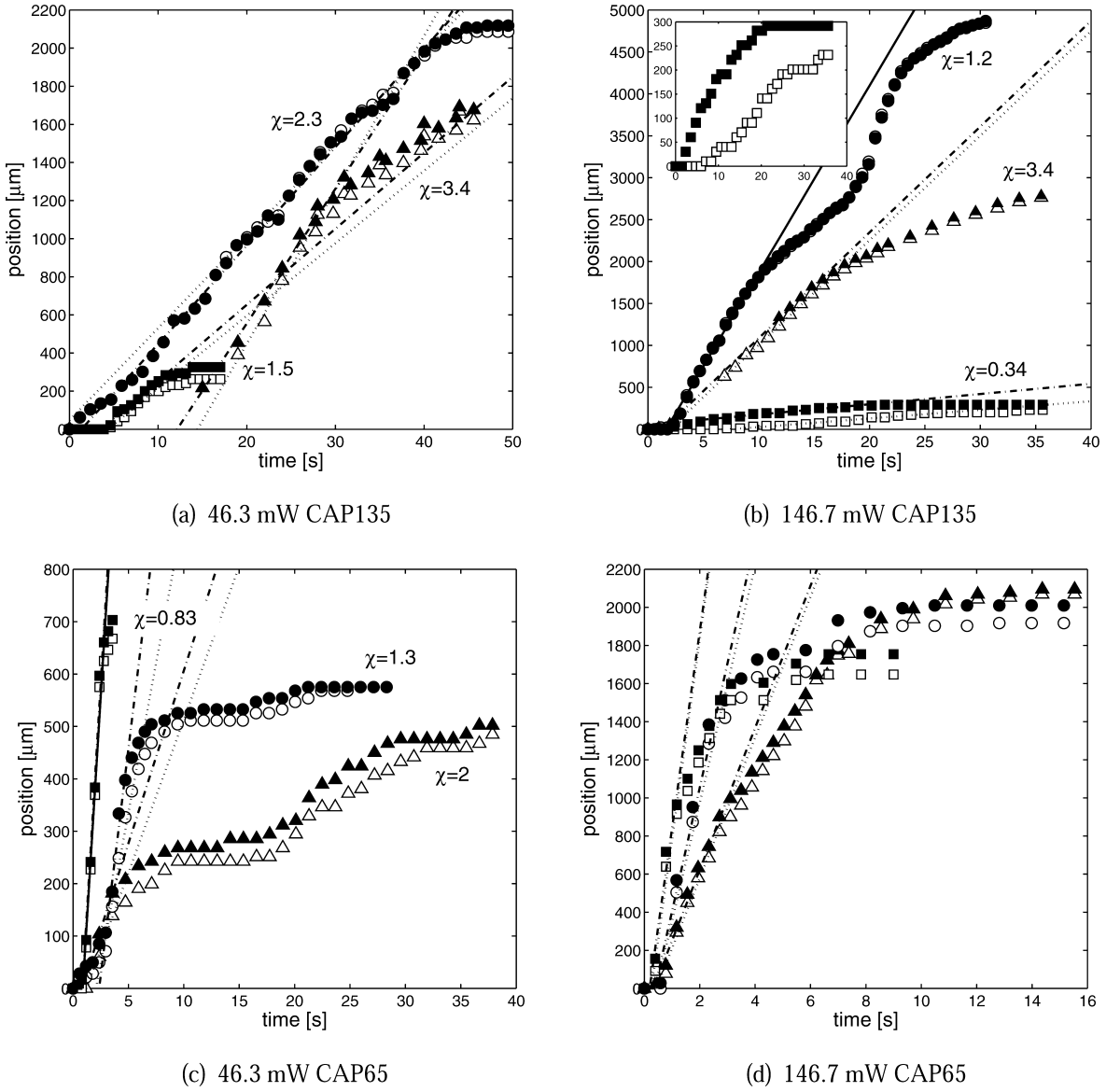

Figure 7. Position of the menisci as a function of time for three different values of the thickness ratio χ and two optical power values; the filled symbols denote the advancing meniscus, and the empty symbols denotes the receding one. The inset in b is an enlarged view of the values corresponding to χ = 0.34. (d) Legend for the symbols the same as in part c. The lines correspond to the maximum velocity, the dotted line corresponds to the receding meniscus, and the dotted−dashed line corresponds to the advancing meniscus. For the CAP135 capillaries (top panel), data correspond to capillaries coated with the multilayer procedure except for χ = 3.4, whose composite layer thickness was achieved with a surface instability. For the CAP65 capillaries (bottom panel), all data correspond to capillaries having a patterned array of pearls.

incandescence or emission), the linear relation between optical intensity and drop velocity does not change. For comparison, we also included the case of a CAP135 capillary having surface instabilities (■, U = 8 mm/min, χ = 1.43), in which a maximum velocity of 343 μm/s was observed. The drop velocities achieved in the last case were very similar to that seen for capillaries having complete coating with a similar thickness (squares and triangles in Figure 8, droplet displacements are also similar between both cases).

The drop velocity as a function of the optical intensity for the CAP65 capillaries, with all having a periodic array of composite pearls, is shown in Figure 9. As in the previous case, the velocity increases linearly with the optical intensity. This time, however, the linear trend can be well distinguished among capillaries coated at different velocities. For instance, for the same optical intensity of 773 W/cm^2, we can have a drop velocity of 62 μm/s with the capillary coated at 24 mm/min (χ = 130 μm/65 μm = 2), a drop velocity of 144 μm/s with the capillary coated at 8 mm/min (χ = 87 μm/65 μm = 1.3), and a drop velocity of 346 μm/s with the capillary coated at 4.61 mm/min (χ = 54 μm/65 μm = 0.83). This feature is perhaps the most important contribution of the present investigation: if we have an optofluidic device working at a certain optical power, we can have a variety of drop velocities in different channels if we adjust, by design, the thickness of the photoresponsive material with Rayleigh−Plateau instabilities. An additional benefit is that the maximum thickness and spacing between pearls is self-adjusted for different capillary diameters. We need to stress as well, in spite of these new design parameters, that the other important variable to take into account in this case is the drop displacement because the drop needs to reach the next perturbation (pearl) in order to continue with its motion. We

dx.doi.org/10.1021/la404221p | Langmuir 2014, 30, 5326−5336

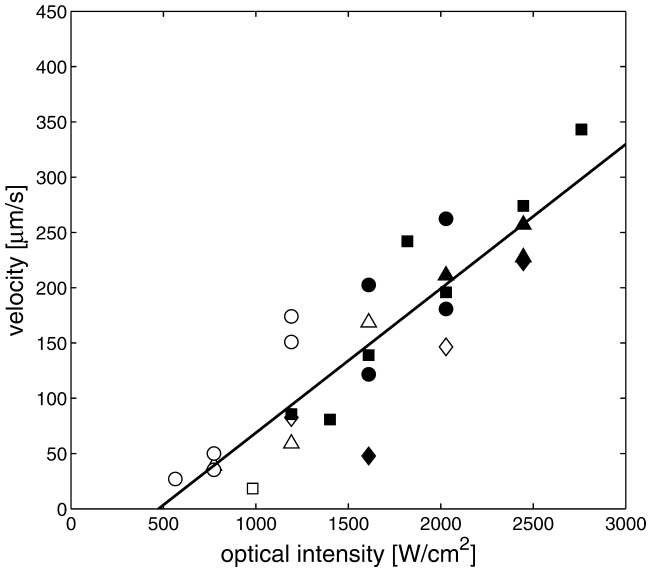

Figure 8. Maximum mean drop velocity as a function of the optical intensity for CAP135 capillaries coated via the multilayer procedure for different ranges of the layer thickness h. Empty symbols, incandescence absent; filled symbols, presence of incandescence at the surface of the composite layer; (◇), χ = 0.95−1.39; (Δ), χ = 1.39−1.84; (○), χ = 1.84−2.28; (□), CAP135 exhibiting surface instabilities, χ = 1.43, U = 8 mm/min. The solid line is a linear fitting for all data.

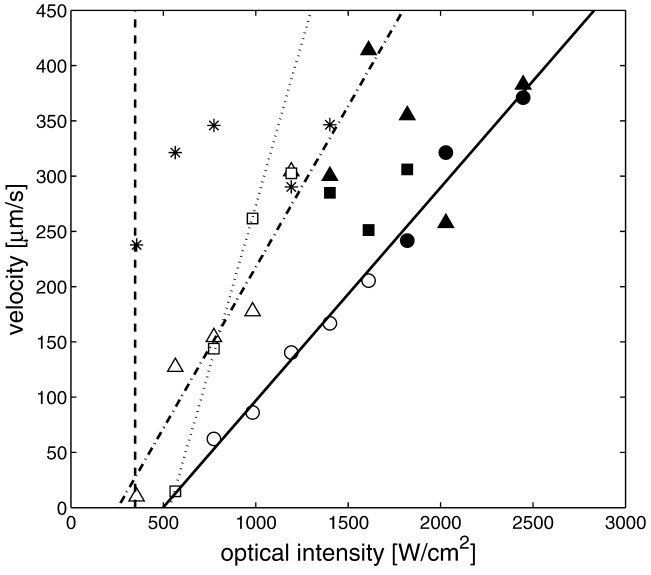

Figure 9. Maximum mean drop velocity as a function of the optical intensity for CAP65 capillaries. Empty symbols, incandescence absent; filled symbols, presence of incandescence at the surface of the composite layer; (○), U = 24 mm/min and χ = 2; (Δ), U = 16 mm/min and χ = 2.3; (□), U = 8 mm/min and χ = 1.3; (*), U = 4.61 mm/min and χ = 0.83, with no incandescence observed for this case. The solid, dotted−dashed, and dotted lines are linear fittings for the first three cases, respectively. The vertical dashed line denotes the calculated minimum optical intensity, I_{min} = 347 W/cm^2, necessary to move the drop corresponding to a contact angle hysteresis of $\cos\theta_R - \cos\theta_A = 7.8 \times 10^{-3}$.

saw that this can be achieved at high power intensities (see Figure 6b).

Another important difference between the wider capillary, CAP135, and the thinner one, CAP65, is that we observed a velocity saturation for the latter after certain optical intensity values and composite thickness h (see Figure 9). As discussed below, this is likely to be due to the finite dimensions of the perturbations and the capillary size. This feature can potentially be used as well to control the drop velocity, although this characteristic has yet to be improved because at high optical intensities the velocity has large variations, especially when $h < H$ and when incandescence is present.

DISCUSSION

Heat transfer in solid materials can occur by conduction and/or radiation (emission), and their relative importance is given by the parameter N (eq 7). In order to estimate N at room temperature (27 °C), we need to provide a value of the thermal conductivity k and the absorption coefficient κ_{abs} of the photoresponsive material. In our case, we can consider the thermal properties of the PDMS to be[22] C_p = 1460 J/kg·K and k = 0.17 W/m·K (although a slight increase in k is expected to occur due to the addition of carbon nanopowder; see for example Hana and Fina[44]). An absorbance coefficient has been estimated by Mercatelli et al.[45] for single-walled carbon nanohorn suspensions in water and ethylene glycol (λ = 632.8 nm, particle size 0.05 to 0.1 μm, κ_{abs} = 11.4 mm^{-1} per g/L) and by Bertocchi et al.[46] for carbon black clouds (λ = 532 nm, particle size 0.57 to 7.2 μm, $\kappa_{abs} \approx$ 5.36 mm^{-1} per g/L). Taking a value of $\kappa_{abs} \approx$ 20 mm^{-1} (our particle concentration is 2.3 g/L), the conduction-to-radiation parameter results in $N \approx$ 500, the optical length range is on the order of $\tau_\lambda \approx$ 20 mm^{-1} × (0.046 to 0.46 mm) = 0.92 to 9.2. Therefore, if the medium is at room temperature, the heat transfer is clearly dominated by conduction. To be more specific, $N \approx 1$ when the temperature of the medium rises to ∼2300 °C. (An analysis of the chemical and physical changes that occurs in the PDMS-carbon composite around these temperatures can be seen in Hautefeuille et al.[47]) The linear relation between the velocity and the optical intensity seen in Figures 8 and 9 confirms the dominance of the conductive regime. It has been shown theoretically[35] and numerically[48] that even when conduction and radiation modes are equally activated (i.e., N = 1) the temperature profile is very close to the limit $N \to \infty$ for τ_λ = 1 in problems where the temperature at the boundaries is prescribed. We think this explains why the appearance of incandescence at the surface at high optical powers does not change the linear relationship between the drop velocity and optical intensity: when emission appears at the surface, half of it is convected into the air while the other half is rapidly absorbed and diffused in the composite layer. We have to mention, however, that we did observe velocity blasts, up to 1 mm/s, when incandescence appeared in the cases of the smallest layer thickness, χ = 0.83 (h = 54 μm) and χ = 1.3 (h = 87 μm), in the CAP65 capillaries. With regard of the velocity saturation seen in Figure 9 for the χ = 0.83, 1.3, and 2.3 cases, this is likely to be due to the finite dimensions of the heat-generation zone and the fast response times of the drop (rapid departure from the heat-generation zone) due to the capillary size and wall thickness. (Note that no velocity saturation was observed for the CAP135 capillary having surface instabilities, Figure 8.) In order to validate this conjecture, one will require a solution of the evolution of the temperature profiles in the composite pearls having different sizes.

dx.doi.org/10.1021/la404221p | Langmuir 2014, 30, 5326−5336

We now proceed to rationalize the linear regime seen in Figures 8 and 9 relating $v \propto I_o$ to the more familiar Fourier relation $v \propto \Delta T$. The physical properties of the mineral oil and solid substrates (PDMS and borosilicate glass) used in following calculations are ρ = 838 kg/m^3, μ = 26 mPa·s, a = 40.71 mN/m, b = 0.221 mN/m °C, and θ_R = 47.6° (in contact with glass) for mineral oil;[26] ρ = 965 kg/m^3, k = 0.17 W/m·K, C_p = 1460 J/kg·K, and $\alpha = 1.2 \times 10^{-3}$ cm^2/s for PDMS;[22] and ρ = 2230 kg/m^3, k = 1.14 W/m·K, C_p = 750 J/kg·K, and $\alpha = 6.81 \times 10^{-3}$ cm^2/s for borosilicate glass.[48b] As a case study, we are going to use the data obtained for the CAP65 capillary having χ = 2 (h = 130 μm, U = 24 mm/min, see Figures 5 and 9).

The temperature difference required to increase the velocity v is obtained with eq 2 using d = 200 μm and the drop length L = 3.9 mm:

$$\frac{v}{\Delta T} = \frac{4}{32}\frac{d}{L}\frac{b\cos\theta_R}{\mu} = 36.7\ \mu\text{m/s °C} \tag{11}$$

As a reference, Sammarco and Burns[26] obtained for equal physical parameters (mineral oil) but different geometry (rectangular cross-section with a width ≈ 50 μm, L ≈2.2 mm) a slope of 7.74 μm/s °C. This is to be expected since for smaller channels the hydrodynamic resistance increases and therefore a larger temperature gradient is needed in order to increase the velocity by the same amount. To see how the slope $v/\Delta T$ can be related to the experimental value v/I_o obtained in Figure 9 [0.1929 (μm/s)(cm^2/W)] by virtue of the Fourier law, we need to calculate the time that the composite−glass layers spend to increase $T(z, t)$ to the value set by the hydrodynamic resistance given a surface optical intensity of I_o. The full solution of this problem will require a complete numerical formulation; alternatively, we can offer an approximate expression for $\Delta T = CI_0 f(z, t)$, where C is a constant that depends on the thermal properties of the material, using the analytical solutions for semi-infinite solids provided by Carslaw and Jaeger.[49] Such a solution for the transport heat equation may fit real values only for early times in the heat diffusion (i.e., during the heat front advance along the material, which scales as $\sim h^2/\alpha$ = 140 ms). We also assumed that heat convection in the air at early times and beam reflectivity are negligible. Considering the perfect thermal contact between the PDMS and glass, we can calculate the temperature increment in two parts: first for the PDMS + carbon composite at z = 130 μm (the thickness of the composite layer placed in front of the optical fiber) and then for the glass layer at z = 195 μm (the thickness of the capillary wall is 65 μm). If the composite is considered to be a nontransparent material (i.e., all of the optical power I_o is absorbed at the surface), then $\Delta T(z, t) = T - T_{ref}$ is given by[49]

$$\Delta T|_{z=130\ \mu\text{m}} = \frac{2I_0}{k}\left[\left(\frac{\alpha t}{\pi}\right)^{1/2} e^{-z^2/4\alpha t} - \frac{z}{2}\,\text{erfc}\left(\frac{z}{2\sqrt{\alpha t}}\right)\right] \tag{12}$$

where erfc is the complementary error function. Wendlandt[50] modified this solution in order to include the absorption coefficient κ_{abs} (i.e., when the material is considered to be semitransparent and light enters the medium, giving an effective heat source per unit volume of $S(z)[\text{W/m}^3] = \kappa_{abs} I_o e^{-\kappa_{abs} z}$, note that we are neglecting the scattering contribution); $\Delta T(z, t)$ then takes the form

$$\Delta T|_{z=130\ \mu\text{m}} = \frac{\kappa_{abs} I_o}{2\rho C_p}\int_0^t \left[e^{\kappa_{abs}{}^2\alpha x + \kappa_{abs} z}\,\text{erfc}\left(\kappa_{abs}(\alpha x)^{1/2} + \frac{z}{(4\alpha x)^{1/2}}\right) + e^{\kappa_{abs}{}^2\alpha x - \kappa_{abs} z}\,\text{erfc}\left(\kappa_{abs}(\alpha x)^{1/2} - \frac{z}{(4\alpha x)^{1/2}}\right)\right] dx \tag{13}$$

Equations 12 and 13 are used to estimate $\Delta T(t)$ at a fixed depth z = 130 μm. The temperature profile in the glass layer at the total depth of 195 μm can be estimated using the relation[49]

$$\Delta T|_{z=195\,\mu\text{m}} = \frac{z}{2\sqrt{\alpha\pi}}\int_0^t \Delta T(t')|_{z=130\ \mu\text{m}} \frac{e^{-z^2/4\alpha(t-t')}}{(t-t')^{3/2}}\,dt' \tag{14}$$

Since ΔT is proportional to the optical intensity I_o, we just have to know the time t necessary to fit the required $u/\Delta T$ (time is the only fitting parameter). After solving the integrals in eqs 13 and 14 numerically and using the approximate expression for $\Delta T|_{z=130\ \mu m} \approx At^B$ in eq 14, we found that the time required to reach the appropriate ΔT at a total depth of 195 μm is 13.8 ms when considering the material to be nontransparent. Similarly, we obtained a value of 3.05 ms for the case when the composite is considered to be semitransparent, having an absorption coefficient of 20 mm^{-1}. Interestingly, the time needed to increase the temperature at a fixed depth is lower—on the order of milliseconds—if light penetrates the material, yielding a distribution of heat sources inside of it.

Up to this point, we have used analytical expressions for the heat transfer to estimate the time required to increase the temperature at a fixed depth and relate the experimental v/I_o to the calculated $v/\Delta T$; however, we still need to calculate the nontrivial contribution of ΔT_{min} (i.e., the contribution of the contact angle hysteresis). Sammarco and Burns[26] determined the advancing and receding contact angles by measuring the pressure needed to advance and retract a meniscus in a channel submerged in mineral oil. Here we estimate $\cos\theta_R - \cos\theta_A$ appearing in the second term of eq 2 by employing eq 8 and the value of ϕ = 2° found in the sessile drop experiments. Considering the physical properties for mineral oil, L = 3.9 mm, d = 200 μm, and a reference temperature of 27°, we found a y-intercept value of −67 μm/s, which corresponds to I_{min} = 347 W/cm^2 after using the slope 0.1929 (μm/s)(cm^2/W); the theoretical line is shown in Figure 9, in good agreement with the experiments. It is remarkable that even a small contact angle hysteresis ($\cos\theta_R - \cos\theta_A = 7.8 \times 10^{-3}$, the value found by Sammarco and Burns[26] was 2.8×10^{-2} for mineral oil) yields a considerable displacement of the $I_o - v$ curves.

■ CONCLUSIONS AND PERSPECTIVES

The thermocapillary flow of single mineral oil drops inside capillaries was induced by irradiating an absorbing material (PDMS + carbon nanopowder) with a laser diode coupled with an optical fiber. Unlike in previous works, the strategy followed here was to coat the capillaries with the composite using fiber-coating techniques. Maximum drop speeds were found to be on the order of ∼300 μm/s below the incandescence threshold and maximum displacements of around 120% of the drop length. As in previous reports,[26,51] the contact angle hysteresis $\Delta\theta$ was found to be a relevant factor to start the drop motion.

dx.doi.org/10.1021/la404221p | Langmuir 2014, 30, 5326−5336

The tilted drop technique was used to infer $\Delta\theta$ for different solid−liquid interfaces; the glass−mineral oil pair was selected due to the relatively low values of $\Delta\theta$. Two coating strategies were used to cover the capillaries with the photoresponsive material: a multilayer procedure using low coating speeds and a single coating step at high speeds to induce the Rayleigh−Plateau instability. For the first case we achieved complete coverage of the capillaries, and high droplet displacements were also achieved; however, poor velocity selectivity was obtained as a function of the composite layer thickness h. For the second case, we obtained a periodic array of pearls of the composite material along the capillary. This time, good velocity selectivity was achieved as a function of the thickness h, probing the fact that the design of a periodic array of heaters via surface instabilities provides a new strategy for obtaining several drop velocities in a single devices having a single optical intensity input. In both cases, a linear relationship between the optical intensity and the drop velocity v was found for a wide range of optical powers, denoting a heat conduction regime.

One important drawback of the experiments shown here is the appearance of incandescence at high optical powers. Although its appearance does not necessarily reflect a change in the velocity−optical intensity plot, in the long term it reduces the mass of photoresponsive material and therefore the initial layer thickness of the composite.

It is our hope that the thermocapillary-driven motion proposed here could be used in optofluidic devices, particularly between different microchips, where coated capillaries can be easily constructed and serve as transport units. Further research can be done in this regard, such as the use of several optical fibers placed along the capillary to achieve larger drop displacements (analogous to the circuit board used for metallic heaters), improve light delivery around the triple contact line, explore the use of flexible microtubes, and employ capillaries modified at the inner surface to transport hydrophilic fluids. Other photoresponsive materials and polymers can also be explored to change the light absorption, reduce incandescence, or modify the periodicity of the heaters along the capillary by varying coating parameters such as the viscosity and surface tension. The heat conduction approaches followed in this work also need to be compared to more rigorous models which take into account the 3-D nature of the problem as well as a more detailed expression for the radiative heat equation that considers, for example, the scattering in a medium with embedded particles.

AUTHOR INFORMATION

Corresponding Author

*E-mail: jvelez@iim.unam.mx.

Notes

The authors declare no competing financial interest.

ACKNOWLEDGMENTS

This work was supported by grants PAPIIT IN102112 (DGAPA-UNAM) and 154464 from Conacyt, Mexico.

REFERENCES

(1) Okawa, D.; Pastine, S. J.; Zettl, A.; Fréchet, J. M. J. Surface tension mediated conversion of light to work. *J. Am. Chem. Soc.* **2009**, *131*, 5396−5398.

(2) Baigl, D. Photo-actuation of liquids for light-driven microfluidics: state of the art and perspectives. *Lab Chip* **2012**, *12*, 3637−3653.

(3) Kim, J. Joining plasmonics with microfluidics: from convenience to inevitability. *Lab Chip* **2012**, *12*, 3611−3623.

(4) Valley, J. K.; NingPei, S.; Jamshidi, A.; Hsu, H.-Y.; Wu, M. C. A unified platform for optoelectrowetting and optoelectronic tweezers. *Lab Chip* **2011**, *11*, 1292−1297.

(5) Delville, J.-P.; de Saint Vincent, M. R.; Schroll, R. D.; Chraïbi, H.; Issenmann, B.; Wunenburger, R.; Lasseux, D.; Zhang, W. W.; Brasselet, E. Laser microfluidics: fluid actuation by light. *J. Opt. A: Pure Appl. Opt.* **2009**, *11*, 034015.

(6) Pimentel-Domínguez, R.; Sánchez-Arévalo, F. M.; Hautefeuille, M.; Hernández-Cordero, J. Laser induced deformation in polydimethylsiloxane membranes with embedded carbon nanopowder. *Smart Mater. Struct.* **2013**, *22*, 037001.

(7) Levitsky, I. A.; Euler, W. B.; Karachevtsev, V. A. *Photophysics of Carbon Nanotubes Interfaced with Organic and Inorganic Materials*; Springer-Verlag: London, 2012.

(8) Fang, C.; Shao, L.; Zhao, Y.; Wang, J.; Wu, H. A gold nanocrystal/Poly(dimethylsiloxane) composite for plasmonic heating on microfluidic chips. *Adv. Mater.* **2012**, *24*, 94−98.

(9) Krishnan, M.; Park, J.; Erickson, D. Opto-thermorheological flow manipulation. *Opt. Lett.* **2009**, *34*, 1976−1978.

(10) Ashok, P. C.; Dholakia, K. Optical trapping for analytical biotechnology. *Curr. Opin. Biotechnol.* **2012**, *23*, 16−21.

(11) Chen, Y.-F.; Jiang, L.; Mancuso, M.; Jain, A.; Oncescu, V.; Erickson, D. Optofluidic opportunities in global health, food, water and energy. *Nanoscale* **2012**, *4*, 4839−4857.

(12) Kintses, B.; van Vliet, L. D.; Devenish, S. R.; Hollfelder, F. Microfluidic droplets: new integrated workflows for biological experiments. *Curr. Opin. Chem. Biol.* **2010**, *14*, 548−555.

(13) Baroud, C. N.; de Saint Vincent, M. R.; Delville, J.-P. An optical toolbox for total control of droplet microfluidics. *Lab Chip* **2007**, *7*, 1029−1033.

(14) Jiang, L.; Erickson, D. Light-governed capillary flow in microfluidic systems. *Small* **2013**, *9*, 107−114.

(15) de Saint Vincent, M. R.; Delville, J.-P. Thermocapillary migration in small-scale temperature gradients: Application to optofluidic drop dispensing. *Phys. Rev. E* **2012**, *85*, 026310.

(16) Lou, J. W.; Villarruel, C. A.; Schermer, R. T. Optically activated core flow shifting within a focused flow. *Appl. Phys. Lett.* **2011**, *99*, 054102.

(17) Ohta, A. T.; Jamshidi, A.; Valley, J. K.; Hsu, H.-Y.; Wu, M. C. Optically actuated thermocapillary movement of gas bubbles on an absorbing substrate. *Appl. Phys. Lett.* **2007**, *91*, 074103.

(18) Yang, D.; Piech, M.; Bell, N. S.; Gust, D.; Vail, S.; Garcia, A. A.; Schneider, J.; Park, C.-D.; Hayes, M. A.; Picraux, S. T. Photon Control of Liquid Motion on Reversibly Photoresponsive Surfaces. *Langmuir* **2007**, *23*, 10864−10872.

(19) Liu, G. L.; Kim, J.; Lu, Y.; Lee, L. P. Optofluidic control using photothermal nanoparticles. *Nat. Mater.* **2006**, *5*, 27−32.

(20) Kotz, K. T.; Noble, K. A.; Faris, G. W. Optical microfluidics. *Appl. Phys. Lett.* **2004**, *85*, 2658−2660.

(21) Ichimura, K.; Oh, S.-K.; Nakagawa, M. Light-Driven Motion of Liquids on a Photoresponsive Surface. *Science* **2000**, *288*, 1624−1626.

(22) Tjahjono, I. K.; Bayazitoglu, Y. Near-infrared light heating of a slab by embedded nanoparticles. *Int. J. Heat Mass Trans.* **2008**, *51*, 1505−1515.

(23) Weinert, F. M.; Braun, D. Optically driven fluid flow along arbitrary microscale patterns using themoviscous expansion. *J. Appl. Phys.* **2008**, *104*, 104701.

(24) Lamhot, Y.; Barak, A.; Rotschild, C.; Segev, M.; Saraf, M.; Lifshitz, E.; Marmur, A.; El- Ganainy, R.; Christodoulides, D. N. Optical Control of Thermocapillary Effects in Complex Nanofluids. *Phys. Rev. Lett.* **2009**, *103*, 264503.

(25) Verneuil, E.; Cordero, M. L.; Gallaire, F.; Baroud, C. N. Laser-Induced Force on a Microfluidic Drop: Origin and Magnitude. *Langmuir* **2009**, *25*, 5127−5134.

(26) Sammarco, T. S.; Burns, M. A. Thermocapillary Pumping of Discrete Drops in Microfabricated Analysis Devices. *AIChE J.* **1999**, *45*, 350−366.

(27) Sammarco, T. S.; Burns, M. A. Heat-transfer analysis of microfabricated thermocapillary pumping and reaction devices. *J. Micromech. Microeng.* **2000**, *10*, 42−55.
(28) Gao, L.; McCarthy, T. J. Contact Angle Hysteresis Explained. *Langmuir* **2006**, *22*, 6234−6237.
(29) Quéré, D.; Lafuma, A.; Bico, J. Slippy and sticky microtextured solids. *Nanotechnology* **2003**, *14*, 1109−1112.
(30) Chen, Y. L.; Helm, C. A.; Israelachvili, J. N. Molecular Mechanisms Associated with Adhesion and Contact Angle Hysteresis of Monolayer Surfaces. *J. Phys. Chem.* **1991**, *95*, 10736−10747.
(31) de Gennes, P.-G.; Brochard-Wyart, F.; Quéré, D. *Capillarity and Wetting Phenomena Drops, Bubbles, Pearls, Waves*; Springer: New York, 2004.
(32) Quéré, D. Fluid coating on a fiber. *Annu. Rev. Fluid Mech.* **1999**, *31*, 347−384.
(33) Rayleigh, L. On the Instability of Jets. *Proc. London Math. Soc.* **1878**, *10*, 4−13.
(34) Dumbleton, J. H.; Hermans, J. J. Capillary Instability of a Thin Annular layer of Liquid around a Solid Cylinder. *Ind. Eng. Chem. Fundam.* **1970**, *9*, 466−469.
(35) Modest, M. F. *Radiative Heat Transfer*, 2nd ed.; Academic Press: Boston, 2003.
(36) (a) Brewster, M. Q. *Thermal Radiative Transfer and Properties*, 2nd ed.; John Wiley & Sons: New York, 1992. (b) http://www.dowcorning.com/applications/search/default.aspx?R=131EN.
(37) Wu, S. Calculation of interfacial tension in polymer systems. *J. Polym. Sci. C* **1971**, *34*, 19−30.
(38) Quéré, D. Drops at rest on a tilted plane. *Langmuir* **1998**, *14*, 2213−2216.
(39) Tropmann, A.; Tanguy, L.; Koltay, P.; Zengerle, R.; Riegger, L. Completely superhydrophobic PDMS surfaces for microfluidics. *Langmuir* **2012**, *28*, 8292−8295.
(40) Kota, A. K.; Li, Y.; Mabry, J. M.; Tuteja, A. Hierarchically Structured Superoleophobic Surfaces with Ultralow Contact Angle Hysteresis. *Adv. Mater.* **2012**, *24*, 5838−5843.
(41) Chen, W.; Fadeev, A. Y.; Hsieh, M. C.; Öner, D.; Youngblood, J.; McCarthy, T. J. Ultrahydrophobic and Ultralyophobic Surfaces: Some Comments and Examples. *Langmuir* **1999**, *15*, 3395−3399.
(42) Goren, S. L. The instability of an annular thread of fluid. *J. Fluid Mech.* **1962**, *12*, 309−319.
(43) Liao, Y.-C.; Li, Y.-C.; Wei, H.-H. Drastic Changes in Interfacial Hydrodynamics due to Wall Slippage: Slip-Intensified Film Thinning, Drop Spreading, and Capillary Instability. *Phys. Rev. Lett.* **2013**, *111*, 136001.
(44) Hana, Z.; Fina, A. Thermal conductivity of carbon nanotubes and their polymer nanocomposites: A review. *Prog. Polym. Sci.* **2011**, *36*, 914−944.
(45) Mercatelli, L.; Sani, E.; Zaccanti, G.; Martelli, F.; Ninni, P. D.; Barison, S.; Pagura, C.; Agresti, F.; Jafrancesco, D. Absorption and scattering properties of carbon nanohorn-based nanofluids for direct sunlight absorbers. *Nanoscale Res. Lett.* **2011**, *6*, 282.
(46) Bertocchi, R.; Kribus, A.; Karni, J. Experimentally determined optical properties of a polydisperse carbon black cloud for a solar particle receiver. *J. Sol. Energy Eng.* **2004**, *126*, 833−841.
(47) Hautefeuille, M.; Cabriales, L.; Pimentel-Domínguez, R.; Velázquez, V.; Hernández- Cordero, J.; Oropeza-Ramos, L.; Rivera, M.; Carreón-Castro, M.; Grether, M.; López- Moreno, E. New perspectives for direct PDMS microfabrication using a CD-DVD laser. *Lab Chip* **2013**, *13*, 4848−4854.
(48) (a) Mazumder, S. A new numerical procedure for coupling radiation in participating media with other modes of heat transfer. *J. Heat Trans.* **2005**, *127*, 1037−1045. (b) http://www.camglassblowing.co.uk/gproperties.htm.
(49) Carslaw, H.; Jaeger, J. *Conduction of Heat in Solids*, 2nd ed.; Clarendon Press: Oxford, U.K., 1959.
(50) Wendlandt, B. Temperature in an irradiated thermally conducting translucent medium. *J. Phys. D: Appl. Phys.* **1973**, *6*, 657−660.
(51) Brzoska, J. B.; Brochard-Wyart, F.; Rondelez, F. Motions of Droplets on HydrophobicModel Surfaces Induced by Thermal Gradients. *Langmuir* **1993**, *9*, 2220−2224.